
Article:
Doyle, Scott James, Lafleur, Trevor, Gibson, Andrew Robert orcid.org/0000-0002-1082-4359 et al. (3 more authors) (2017) Enhanced control of the ionization rate in radio-frequency plasmas with structured electrodes via tailored voltage waveforms. Plasma sources science & technology. ISSN 0963-0252

https://doi.org/10.1088/1361-6595/aa96e5

Enhanced control of the ionization rate in radio-frequency plasmas with structured electrodes via tailored voltage waveforms

Scott J. Doyle[1], Trevor Lafleur[2], Andrew R. Gibson[1,2], Peng Tian[3], Mark J. Kushner[3], and James Dedrick[1]

[1]York Plasma Institute, Department of Physics, University of York, Heslington, York, YO10 5DD, UK

[2]LPP, CNRS, Ecole Polytechnique, UPMC Univ, Paris 06, Univ. Paris-Sud, Observatoire de Paris, Universite Paris-Saclay, Sorbonne Universites, PSL Research University, 91128 Palaiseau, France

[3]University of Michigan, Dept. of Electrical and Computer Engineering, 1301 Beal Ave., Ann Arbor, MI 48109-2122, USA

[1]E-mail: sjd549@york.ac.uk

November 10, 2017

Abstract

Radio-frequency (rf) capacitively coupled plasmas that incorporate structured electrodes enable increases in the electron density within spatially localised regions through the hollow cathode effect. This enables enhanced control over the spatial profile of the plasma density, which is useful for several applications including materials processing, lighting and spacecraft propulsion. However, asymmetries in the powered and grounded electrode areas inherent to the hollow cathode geometry lead to the formation of a time averaged dc self-bias voltage at the powered electrode. This bias alters the energy and flux of secondary electrons leaving the surface of the cathode and consequentially can moderate the increased localized ionization afforded by the hollow cathode discharge. In this work, two-dimensional fluid-kinetic simulations are used to demonstrate control of the dc self-bias voltage in a dual-frequency driven (13.56 MHz, 27.12 MHz), hollow cathode enhanced, capacitively coupled argon plasma over the 66.6 - 200 Pa (0.5 - 1.5 Torr) pressure range. By varying the phase offset of the 27.12 MHz voltage waveform, the dc self-bias voltage varies by 10-15 % over an applied peak-to-peak voltage range of 600-1000 V, with lower voltages showing higher modulation. Resulting ionization rates due to secondary electrons within the hollow cathode

cavity vary by a factor of 3 at constant voltage amplitude, demonstrating the ability to control plasma properties relevant for maintaining and enhancing the hollow cathode effect.

1 Introduction

The hollow cathode effect (HCE), generated in capacitively coupled plasmas through the use of structured electrodes, offers the capability to locally increase the plasma density. To achieve this, hollow cathode discharges are typically characterized by a cylindrical electrode cavity electrically connected to a larger grounded area and can be operated with radio-frequency[1] (rf) or dc[2] power. They are employed over a wide range of pressures from atmospheric[3] to high vacuum[4–6] and can form part of the gas source[7] or operate external to it[8]. Hollow cathodes are being researched for use in a large variety of industrial processes including etching and deposition[1,9], CO_2 dissociation[10], light sources[11] and spacecraft propulsion[12–14]. For *pd* (pressure × distance) values in the range of 0.01 - 10 Torr cm the hollow cathode effect (HCE) can be initiated, resulting in a large increase in plasma density for a given voltage[2,15].

One of the proposed mechanisms of the HCE arises from the pendular motion of electrons produced within the electrode cavity, resulting in an increased number of ionization events per secondary electron[5]. Positive ions impacting on the inside surface of the hollow cathode produce secondary electrons that are subsequently accelerated through the plasma sheath[16]. These electrons typically have non-thermal 'beam-like' energy distributions with a mean energy much higher than electrons produced through collisions in the plasma bulk. These high energy electrons reflect from the opposite cathode sheath, return to the original sheath, and reflect again leading to pendular motion within the cavity. They predominately slow by ionization collisions which, when coupled with the higher specific power deposition of the pendular motion, produces a high plasma density[5,15]. Hollow cathodes operated at low pressures (≤ 13 Pa) can also enforce higher electron energies by enhancing the maximum sheath expansion within/above the hollow cathode cavities[8]. At higher pressures, where the electron collision frequency is high, pendular electron motion within the cavity is inhibited and collisionless heating at the sheath expansion decreases in efficiency. Under these conditions, control of secondary electron energies via tailoring the sheath voltage drop represents a promising mechanism to control the plasma density in hollow cathodes.

In capacitively coupled plasmas operating at rf voltages, an electrical asymmetry may result when the powered and grounded electrodes have different current collecting areas. This physical asymmetry gives rise to a dc self-bias voltage forming at the powered electrode, which ensures that the time-averaged current reaching each electrode is zero[17]. Implementing a hollow cathode structure into the powered electrode introduces, or exaggerates, this geometrical asymmetry between the powered and grounded electrode surface areas. The formation of a dc self-bias voltage creates challenges for maintaining desired plasma properties as it alters the voltage drop at the powered electrode[18]. A

negative dc bias increases the time averaged voltage drop, while a positive dc bias decreases the time-averaged voltage drop. A reduction in the voltage drop at the powered electrode may decrease the ion energies at the electrode surface, which for sufficiently high ion energy, may reduce the probability of producing secondary electrons[15]. Additionally, for a positive dc bias, secondary electrons are accelerated through a smaller sheath potential, compounding the reduction of the HCE. On the other hand, a negative dc bias will increase both the incident ion energy, which may increase the secondary electron emission coefficient, and will increase the secondary electron energy entering the bulk plasma, which will increase ionization. Both lead to an enhancement in the HCE.

Recent investigations employing hollow cathode geometries in capacitively coupled plasmas[19,20] have operated with a relatively small powered electrode surface area compared to that of the grounded vacuum chamber, ensuring a negative dc self-bias. However, in large scale industrial processes, for example plasma deposition of soft materials, it is often the case that the powered electrode may have the larger area[21,22]. In reactors of this type the implementation of a hollow cathode structure would increase the surface area of the powered electrode, leading to an increasingly positive dc self-bias voltage which inhibits the HCE. It would therefore be beneficial to regulate the dc self-bias voltage and hence more effectively control the formation of the HCE.

The dc self-bias is dependent upon the electrode areas and sheath width asymmetry[23,24], secondary electron emission coefficient asymmetry[25], and electrical asymmetries[26]. Of these, the electrical asymmetry is the only property that does not depend on reactor geometry and material choice and can therefore be controlled for a given reactor configuration.

Introducing non-sinusoidal waveforms can induce an electrical asymmetry effect (EAE), allowing control over the dc self-bias voltage[17]. The application of the EAE to enhance process control in capacitively coupled plasmas has been a topic of growing interest over the last decade[26–28]. Applying a dual-frequency voltage waveform, e.g. the fundamental at frequency ω_0 and first harmonic at frequency $2\omega_0$, allows for the creation of asymmetric waveforms, the specific shape of which can be tailored by varying the phase offset between the fundamental and first harmonic voltages[29]. Varying the phase offset while maintaining the applied waveform amplitude results in a controllable dc self-bias voltage, which has been demonstrated to provide effective control over the ion energy and fluxes to surfaces[30,31]. The application of additional harmonics with specific phase shifts allows for production of sawtooth-like and pulse-like waveforms to enable additional control[32,33].

In this work, we use two-dimensional numerical simulations to demonstrate enhanced control over the dc self-bias in a hollow cathode geometry excited by dual-frequency electrically asymmetric waveforms. Control over the dc self-bias voltage is demonstrated by varying the phase offset between

the fundamental frequency (13.56 MHz) and its first harmonic (27.12 MHz), achieving a maximum variation of one eighth of the peak-to-peak voltage. The model used in this investigation is described in section 2, and results for 1 Torr argon hollow cathode discharges operated with 800 V_{pp} single and dual-frequency waveforms are presented in sections 3.1 and 3.2, respectively. Section 3.3 presents dual-frequency results for a wider range of pressures; 0.5 Torr, 1.0 Torr and 1.5 Torr, and voltages; 600 V_{pp}, 800 V_{pp} and 1000 V_{pp}.

2 Description of the Model

The hollow cathode reactor configuration used in this investigation is illustrated in figure 1. An external circuit comprising of an rf voltage source and blocking capacitor is connected to the powered electrode (not shown in figure 1), where the blocking capacitor prevents a dc current back to the power source and maintains the time averaged dc self-bias voltage on the powered electrode. The voltage waveform, $\phi_{rf}(t)$, is applied either as a single frequency sinusoidal waveform or a dual-frequency non-sinusoidal waveform.

Two-dimensional, fluid-kinetic simulations were undertaken using the Hybrid Plasma Equipment Model (HPEM)[34]. The simulation domain, shown in figure 1, consisted of a cylindrically symmetric chamber 25.5 mm in radius, layered with 3 mm of alumina on the radial and top walls. A gap of 40 mm separates the grounded and powered electrodes, which are 22.5 mm in radius. The powered electrode incorporates two, 10 mm deep cavities spaced 5 mm apart radially. Two cavities and a dielectric layer were employed such that interference from the wall on the inner cavity was minimized. The dielectric layer also acted to shield the grounded side wall from the plasma, and therefore increase the physical symmetry of the reactor. The focus of the investigation was on the inner cavity centred at 5 mm, denoted by the shaded region in figure 1.

Points A (R = 5 mm, Z = 12 mm) and B (R = 5 mm, Z = 20 mm) mark locations from which ionization due to secondary electrons and plasma density were investigated. These were chosen to be representative of conditions within the cavity and in the discharge bulk, respectively.

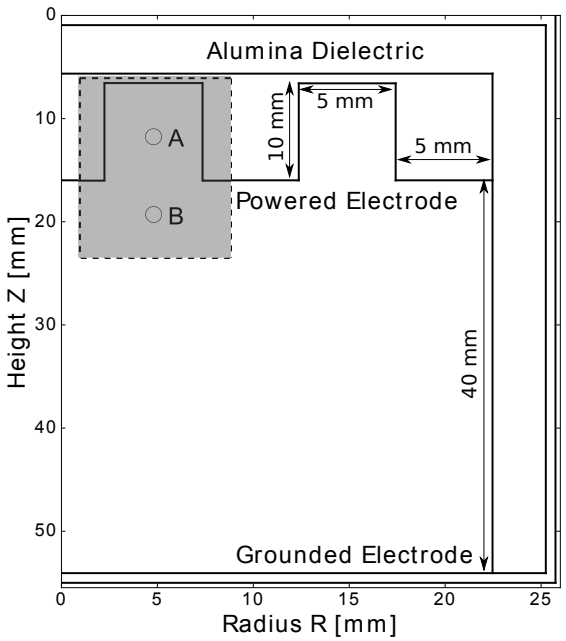

Figure 1: Illustration of the simulation domain (not to scale), radially symmetric around the *Z*-axis. The shaded area shows the region-of-interest where the centre of the hollow cathode cavity and a point representative of the plasma bulk are denoted by A and B, respectively. Z = 0 mm is located in the top-left corner.

The reactor was operated with a fixed pressure of argon at 66.6 Pa, 133.3 Pa, 200 Pa (0.5 Torr, 1 Torr or 1.5 Torr). The discussion of plasma properties in sections 3.1 and 3.2 are for 133.3 Pa (1 Torr), while discussion in section 3.3 addresses all three. The charged particle species included in the simulation are Ar^+, Ar_2^+ and e^-, with secondary electrons solved for separately from electrons created in the plasma bulk. Neutral species included are: Ar, Ar(4s), Ar(4p), Ar(4d) and Ar_2^* where the reaction mechanism is the same as discussed in Ref. 35. All particle species densities, with the exception of secondary electrons, are obtained from the solution to mass, momentum and energy conservation equations. The electron energy distribution function (EEDF) for electrons created in the plasma bulk is determined using the two-term approximation of the Boltzmann equation. At the pressures employed, the plasma is considered to be collisional and therefore the ion and neutral energy distribution functions can reasonably be considered to be Maxwellian. Poisson's equation is solved to obtain the temporally and spatially resolved potential.

Secondary electron emission is introduced through an energy independent model with an emission coefficient of $\gamma = 0.2$ at the powered electrode[15] and $\gamma = 0.0$ at the grounded electrode and dielectric surfaces. It is important to note that the particular values of γ used at powered and grounded electrodes have an influence on the symmetry of the plasma and therefore the value of the dc self-bias. As a result, the magnitude of the effects considered in this work will depend on these values, however, the trends presented are expected to be valid for most realistic values of γ. Ion fluxes are collected on

the powered electrode and a Monte Carlo method is then used to track the trajectories of secondary electrons emitted from the powered electrode in proportion to the ion flux and secondary electron emission coefficient[36]. Secondary electron pseudo-particles are launched at the powered electrode surface with an initial energy of 4 eV and are accelerated through the local potential gradient. As this is the outcome of a Monte-Carlo simulation there are no further assumptions made regarding the shape of the secondary electron energy distribution[37].

Electron-neutral collisions included in the model include elastic, excitation and ionization reactions, the interaction cross-sections for which are obtained from Refs. 38–42, full details are given in Ref. 35. Ion-neutral charge exchange collisions are employed with a rate coefficient of 5.66×10^{-10} cm^{-3} $(T_g/300)^{0.5}$ where T_g is the neutral-gas temperature[43].

Dual-frequency voltage waveforms, constructed through the superposition of 13.56 MHz and 27.12 MHz sinusoids with a variable phase delay, are generated using equation 1 and an example of a dual-frequency waveform is shown in figure 2.

$$\phi_{\mathrm{rf}}(t) = \sum_{k=1}^{n} \left(\frac{\phi_0}{n} \right) \cos(k\omega_0 \mathrm{t} + \theta_k) \tag{1}$$

Here, $\phi_{\mathrm{rf}}(t)$ is the voltage amplitude of the combined waveform, ϕ_0 is the maximum amplitude, $\omega_0 = 2\pi f_0$ is the fundamental angular frequency, θ_k is the k'th harmonic offset and n is the total number of applied frequencies. Here $n = 2$, $\theta_1 = 0$ and $0° < \theta_2 < 360°$, from this point forward θ_2 will be referred to as θ.

Figures 2 (a) and (b) show two examples of dual-frequency waveforms generated using equation 1 with phase offsets of θ =60° and θ =210°, respectively.

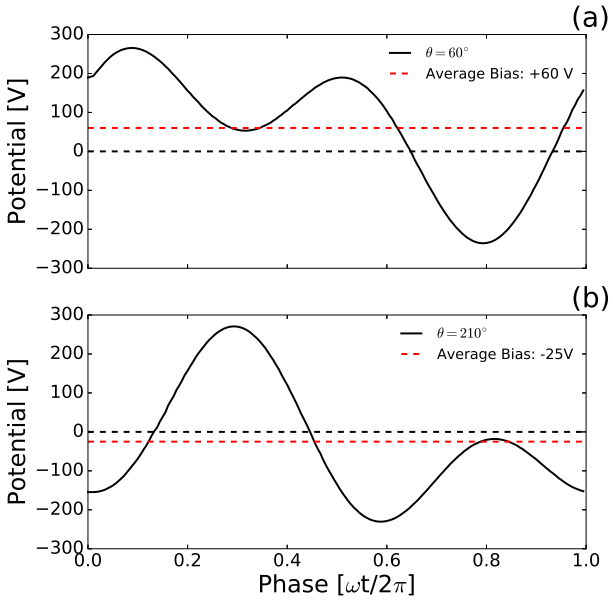

Figure 2: Examples of dual-frequency, 13.56 MHz, 27.12 MHz, waveforms generated using equation 1 with the 27.12 MHz waveform applied with a phase offset θ of (a) 60° and (b) 210°. Zero potential is shown with a black dotted line and the mean of the waveform (denoted as average bias) is shown with the red dotted line.

As the phase offset of the 27.12 MHz harmonic is varied the time-averaged bias of the waveform is altered, this results in a time-averaged electrical asymmetry over an rf cycle and provides a mechanism for controlling the electrode dc self bias voltage. However, due to the phase offset, such asymmetric voltage waveforms do not have a single voltage amplitude, it is therefore often easier to discuss them in terms of the absolute peak-to-peak voltage, V_{pp}, defined as follows:

$$V_{pp} = \max \phi_{rf}(t) - \min \phi_{rf}(t) \tag{2}$$

In sections 3.2 and 3.3 the fundamental frequency 13.56 MHz and first odd harmonic 27.12 MHz were employed, each with an amplitude of $\phi_0/2$ to enable an effective comparison with the single frequency case.

3 Hollow Cathode Effects in a Radio-Frequency Powered Discharge

3.1 Single Frequency Operation

A single frequency control case was performed to confirm the presence of the HCE and establish a baseline for the resulting dc self-bias voltage formation. The control case employed a 400 V amplitude (800 V_{pp}), 13.56 MHz driving voltage and an argon pressure of 133.3 Pa (1 Torr). The time-averaged spatial distributions of the plasma density and ionization rate due to secondary electrons are shown in figure 3 (a) and (b), respectively.

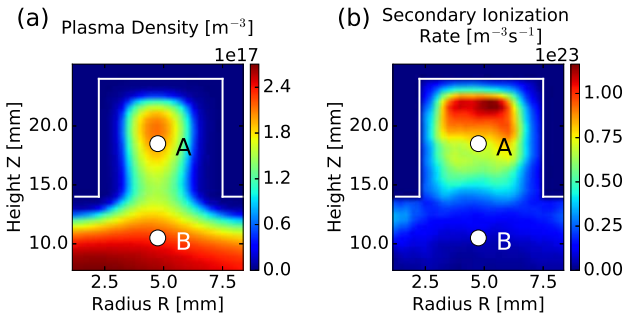

Figure 3: Time-averaged spatial distributions of (a) plasma density and (b) secondary-electron ionization rates in a 133.3 Pa (1 Torr) argon discharge driven by a single-frequency 13.56 MHz voltage waveform at 400 V amplitude (800 V_{pp}). The boundary of the hollow cathode cavity is shown by the solid line.

The time-averaged plasma density shows little variation between the cavity (A) and bulk (B), with maximum values of 2.0×10^{17} m^{-3} and 2.3×10^{17} m^{-3}, respectively. The hollow cathode effect can be observed in figure 3 (b) as an increased rate of ionization by secondary electrons within the cavity region (point A) as compared to the discharge bulk (point B). The powered electrode dc self-bias voltage is 98 V with a peak plasma potential of 224 V. These results qualitatively agree with previous particle-in-cell simulations using a similar reactor configuration at 34 Pa (0.258 Torr)[15].

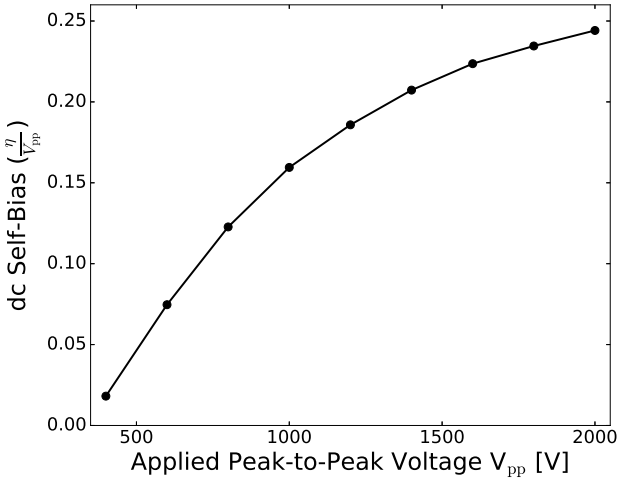

Figure 4: Normalized powered electrode dc self-bias voltage with respect to applied voltage amplitude. Single-frequency operation at 13.56 MHz, in 133.3 Pa (1 Torr) of argon.

The dc self-bias voltage η, normalized to V_{pp}, increased for increasing applied voltage amplitude as shown in figure 4. This trend is consistent with a previously developed analytical model as summarized in equation 3[17]:

$$\eta = -\frac{1-\epsilon}{1+\epsilon}\phi_0 \qquad \text{where } \epsilon \propto \left(\frac{A_p}{A_g}\right)^2 \frac{\bar{n}_{sp}}{\bar{n}_{sg}} \tag{3}$$

where ϕ_0 is the voltage waveform amplitude, ϵ is the symmetry parameter, A_p and A_g are the

powered and grounded electrode surface areas, and $\bar{n}_{sp}$ and $\bar{n}_{sg}$ are the spatially averaged ion densities in the powered and grounded sheaths, respectively. For a single frequency discharge the symmetry parameter, and hence dc self-bias voltage, increases due to the increasing asymmetry in ion density between the powered and grounded electrode sheaths.

Note that the dc self-bias in equation 3 is defined with respect to the voltage waveform amplitude, however results presented here are normalized to V_{pp}. This is necessitated as asymmetric waveforms do not have a single voltage amplitude. The result is that the dc self-bias is normalized from -0.5 $\leq \eta \leq$ 0.5, as opposed to -1 $\leq \eta \leq$ 1.

As the ratio of the dc self-bias voltage to applied voltage increases, and the dc self-bias is positive, the resulting normalized voltage drop through the powered electrode sheath decreases as shown in figure 5.

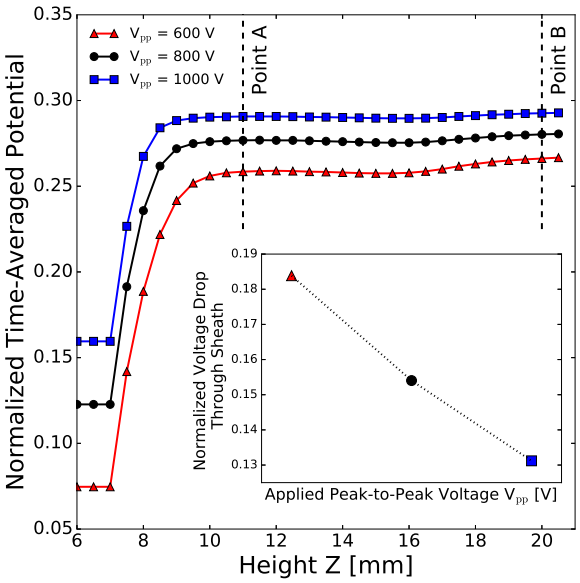

Figure 5: Plasma potential profiles along the inner cavity central axis (R = 5 mm), normalized to V_{pp}, with respect to applied voltage amplitude. Inset displays normalized voltage drop from point A to the electrode surface (Z = 7 mm) for the voltage amplitudes shown. Single-frequency operation at 13.56 MHz, 133.3 Pa (1 Torr) argon.

This decrease in sheath voltage drop reduces the HCE through a decrease in the acceleration of secondary electrons through the powered electrode sheath. Since the dc self-bias voltage increases with increasing applied voltage amplitude, this behaviour limits the range of applied voltages for a given reactor geometry for which the HCE can be effectively employed when operated using a single frequency.

3.2 Dual-Frequency Operation

To increase control over the HCE through regulation of the dc self-bias voltage two driving frequencies, 13.56 MHz and 27.12 MHz, were applied to the powered electrode using the waveform of equation 1. The applied voltage amplitude was maintained at 400 V, however due to the phase shift between the two harmonics they add such that $V_{pp} \leq 800$ V. The resulting variation in the dc self-bias voltage, secondary electron ionisation rate and electron density within the cavity (point A) and bulk (point B) with respect to first harmonic phase offset θ are shown in Figure 6.

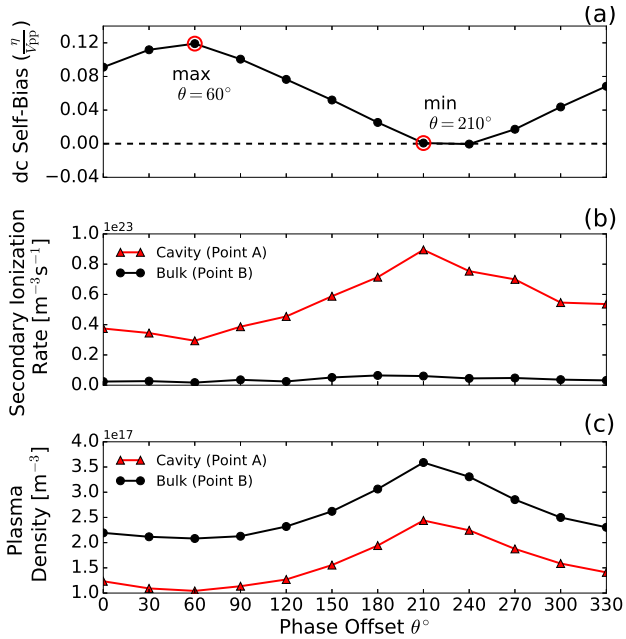

Figure 6: Variation in (a) normalized powered electrode dc self-bias voltage, (b) ionisation rate due to secondary electrons and (c) plasma density as a function of first harmonic phase offset within the hollow cathode cavity (point A) and in the discharge bulk (point B). The dashed line in figure (a) represents zero dc self-bias voltage, solid lines added for clarity.

Figure 6 (a) shows that the powered electrode dc self-bias voltage varies approximately sinusoidally with respect to θ. Note that the dc self-bias has been reduced to approximately zero for phase angles of 210° and 240°. The difference between the maximum and minimum self-bias, indicated by the red circles, is 96 V, corresponding to approximately 1/8 V_{pp}. The waveforms resulting in the most positive and negative dc self-bias voltages, $\theta = 60°$ and $\theta = 210°$, are shown in figures 2 (a) and (b), respectively. This trend in dc self-bias modulation qualitatively agrees with a previous analytical model making use of a physically symmetric geometry[26,44]. The variation in dc self-bias voltage is not symmetric about zero due to the existing physical asymmetries within the reactor[44].

Figure 6 (b) and 6 (c) show the secondary electron ionization rates and plasma density at points A and B as a function of the phase offset between the 13.56 MHz and 27.12 MHz voltage waveforms. The maximum values for plasma density and secondary electron ionization rate both coincide with the minimum dc self-bias voltage of −0.4 V at $\theta = 210°$ phase offset. This trend is expected as the

secondary electrons emitted will appear at the bottom of a larger potential well if the electrode has a less positive bias, and will be subsequently accelerated to higher energies resulting in a higher power coupling efficiency to the electrons. Further, the higher energy secondaries are more efficient ionizers, not only penetrating deeper into the bulk plasma but also capable of generating a greater number of ionization events. As previously described, the fraction of the waveform for which the voltage is less than zero decreases as the dc self-bias becomes more positive. It follows that the least positive self-bias voltage, i.e. $\theta = 210°$ in Figure 6 (a), will correspond to the largest number of secondary electrons with sufficient energy to contribute to the HCE.

Contour plots of the plasma densities at the extrema in dc self-bias voltage, $\theta = 60°$ and $\theta = 210°$, respectively, are shown in figure 7 (a) and (b) and the corresponding secondary electron ionization rates are shown in 7 (c) and (d).

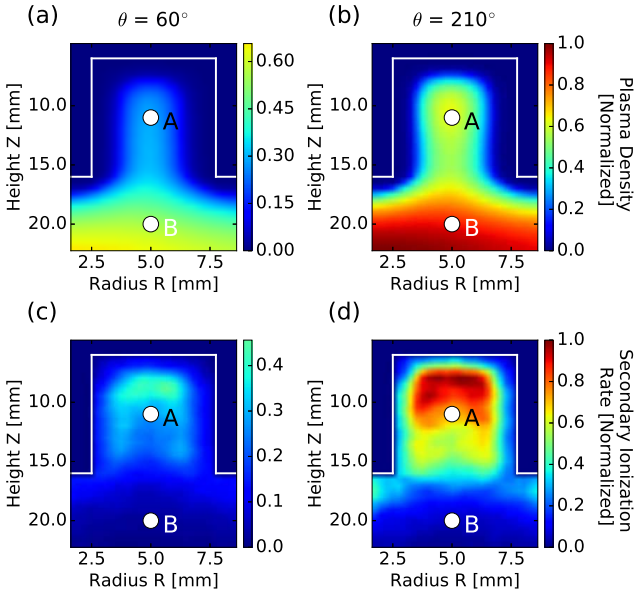

Figure 7: Spatial distributions of time-averaged plasma density for (a) $\theta = 60°$ and (b) $\theta = 210°$ and ionization rates due to secondary electrons at (c) $\theta = 60°$ and (d) $\theta = 210°$. Images are normalized to maximum value in the $\theta = 210°$ case where, $\theta = 60°$ and $\theta = 210°$ represent the minimum and maximum dc self-bias voltages, -0.4 V and $+95$ V, respectively shown in figure 6 (a). Dual-frequency operation at 800 V_{pp} with 133.3 Pa (1 Torr) argon.

The secondary electron ionization rates in the cavity, at point A, vary by a factor of 3 as the phase offset is varied over $0° < \theta < 360°$, reaching a maximum of 9.0×10^{22} m^{-3} at 210° offset. Secondary electron ionization rates outside the cavity, point B, are not significantly influenced by the variation in dc self-bias voltage, remaining at approximately 1.7×10^{22} m^{-3}s^{-1} for all phase angle offsets, shown previously in figure 6 (b).

In figures 7 (d) and (b) it should be noted that although the peak secondary ionization rate was found within the cavity at point A, the peak plasma density was found within the discharge bulk at point B. The plasma density within the cavity and within the bulk follow a similar trend to the

secondary electron ionization rate, reaching a maximum value at $\theta = 210°$, corresponding to the minimum dc self-bias voltage. The maximum plasma density at point B increases to 3.6×10^{17} m^{-3} at $\theta = 210°$ and is modulated by 40 % over the full range of phase offsets.

Argon ion (Ar^+) density profiles, centered along the inner cavity central axis (R = 5 mm), between the powered and grounded electrodes are shown in figure 8 for 13.56 MHz operation and dual-frequency operation at the maximum and minimum dc self-bias voltages, $\theta = 60°$ and $\theta = 210°$, respectively.

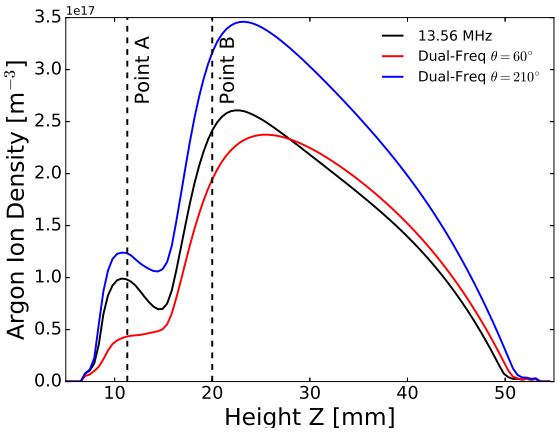

Figure 8: Time-averaged argon ion (Ar^+) density profiles centered along the inner cavity central axis (R = 5 mm) for single frequency 13.56 MHz operation, and dual-frequency operation with $\theta = 60°$ and $\theta = 210°$, where, $\theta = 60°$ and $\theta = 210°$ represent the minimum and maximum dc self-bias voltages, −0.4 V and +95 V, respectively. Performed at 800 V_{pp} with 133.3 Pa (1 Torr) argon.

A localized increase in argon ion density within the cavity at point A (Z = 12 mm) can be observed as well as an increase in the density in-front of the powered electrode at point B (Z = 20 mm) where the density peaks at approximately Z = 25 mm. The enhanced argon ion densities achieved for the, most negative, 210° case can be seen to extend until the grounded electrode surface at Z = 55 mm. The extent of the enhancement is greatest between 15 mm ≤ Z ≤ 30 mm.

Note that, although performed at approximately constant peak-to-peak voltage, the power deposited varies by 32 % over the range of phase offsets. Resulting argon ion densities vary by 60 % in the HC cavity (point A) and 40 % in the discharge bulk (point B) respectively.

3.3 Voltage and Pressure Dependence

The first harmonic phase offset was varied as described in section 3.2 for values of V_{pp} of 600 V, 800 V and 1000 V at a fixed pressure of 133.3 Pa (1 Torr) and also for pressures of 66.6 Pa, 133.3 Pa, 200 Pa (0.5 Torr, 1 Torr or 1.5 Torr) at a fixed V_{pp} of 800 V; the results of which are shown in figure 9:

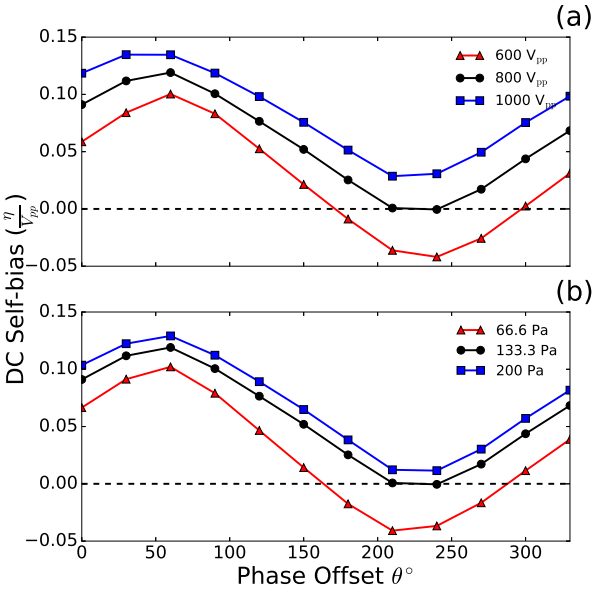

Figure 9: Normalized powered electrode dc self-bias voltage as a function of first harmonic phase offset for varying (a) applied peak-to-peak voltage and (b) argon pressure. The dashed lines represent zero dc self-bias voltage, solid lines added for clarity. Dual-frequency operation, Pressure varied for V_{pp} = 800 V, Voltage varied for a pressure of 133.3 Pa (1 Torr).

An increase in V_{pp} results in a higher average dc self-bias, this agrees with the single frequency case shown in figure 4. The achievable modulation in dc self-bias is 14.2 % at 600 V_{pp} as compared to 12.0 % at 800 V_{pp} and 10.6% at 1000 V_{pp} suggesting that the EAE is more pronounced at lower voltages. This variation in the modulation is found to be approximately linear for changes in voltage which suggests that it may be dominated by variation in the sheath width asymmetry between the powered and grounded electrode as described in equation 3.

The effects of varying reactor pressure, figure 9 (b), show that increased pressures result in more positive dc self-biases. The dc self-bias modulations are 14.3 % at 66.6 Pa (0.5 Torr), 12.0 % at 133.3 Pa (1.0 Torr) and 11.8 % at 200 Pa (1.5 Torr). The decrease in achievable modulation with increasing pressure is not as pronounced as with increasing voltage. The change in modulation varies non-linearly with pressure, with a sharp change in modulation observed between 133.3 Pa (1.0 Torr) and 66.6 Pa (0.5 Torr) where the dc self-bias becomes negative.

The secondary ionization rate increases for increasing pressure as can be seen in figures 10 (a) and (b). The spatial distribution of secondary ionization moves from the centre of the hollow cathode at low pressures to near the surface of the electrode (Z = 7 mm) at higher pressures.

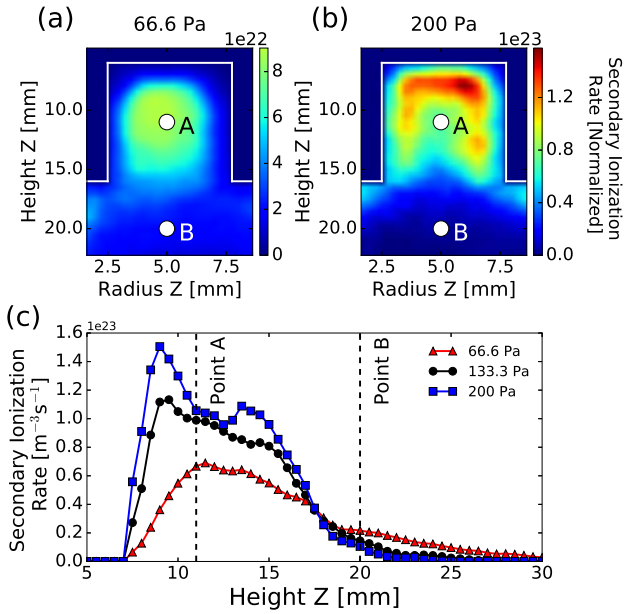

Figure 10: Spatial distributions of time-averaged secondary ionization rates at $\theta = 210°$ for (a) 66.6 Pa (0.5 Torr) and (b) 200 Pa (1.5 Torr). Profiles of the secondary ionization rates along the inner cavity central axis (R = 5 mm) are shown in (c) for varying reactor pressures. Dual-frequency operation at 800 V_{pp}.

The location of maximum secondary ionization rate can be seen more clearly in 10 (c). These locations are 11.5 mm, 9.5 mm and 9 mm for 66.6 Pa, 133.3 Pa, 200 Pa (0.5 Torr, 1 Torr or 1.5 Torr) respectively. The magnitude of the ionization rate and the location of peak ionization both change most between 66.6 Pa and 133.3 Pa. This correlates with the large difference in the dc self-bias between these two pressures, as compared to 133.3 Pa and 200 Pa, shown in figure 9 (b). The peak in secondary ionization rate is also much more pronounced for 133.3 Pa and and 200 Pa than the lower 66.6 Pa case. This is attributed to the decreased electron mean free path at these pressures, with the region of peak ionization shifting from the centre of the cavity to just beyond the sheath edge in figure 10 (b). However, distances beyond Z = 17 mm in the bulk region show the opposite trend in secondary ionization, which is observed to increase with decreasing pressure. This is attributed to an increased electron mean-free path at lower pressures leading to a reduced diffusive (collisional) confinement within the cathode.

The increase in secondary ionization rate with increasing pressure arises from a combination of a reduced secondary electron mean-free path $\lambda_d \propto n_{\mathrm{Ar}}^{-1}$ and a reduced sheath width $S_x \propto n_{\mathrm{Ar}}^{-0.5}$ at higher pressures, where S_x is the sheath width[23]. This non-linear relationship between pressure and secondary ionization rate within the hollow cathode cavity will lead to a non-linear change in the relative plasma densities at the powered and grounded electrode surfaces as described by the symmetry parameter ϵ in equation 3. This explains the non-linear dc self-bias modulation observed for changes in pressure, figure 9 (b), as compared to changes in voltage, 9 (a).

4 Conclusions

Two-dimensional, fluid-kinetic simulations have been undertaken to investigate a capacitively coupled, hollow cathode enhanced discharge driven by a dual-frequency voltage waveform. Control over the dc self-bias voltage has been demonstrated by varying the phase offset between the fundamental frequency (13.56 MHz) and 1st harmonic (27.12 MHz). This is in contrast to discharges driven by single rf frequencies where only limited control can be achieved for a constant peak-to-peak voltage. The dc self-bias modulation was found to vary by 10-15 % over an applied peak-to-peak voltage range of 600-1000 V. This modulation was found to decrease approximately linearly with increasing voltage and decrease non-linearly with increasing reactor pressure. Resulting secondary ionization rates within the cavity can be regulated by a factor of 3 and plasma densities were demonstrated to increase by 40 % over a 360° range of phase offsets. As a result of the enhanced control over the dc self-bias voltage, and resultant ionization rate, increased flexibility in the design of plasma processing reactors is achieved through the hollow cathode effect.

5 Acknowledgements

The authors would like to thank Timo Gans, Erik Wagenaars, Christopher Murphy and Peter Hill for useful discussions. The work presented herein was funded by the Engineering and Physical Sciences Research Council (EPSRC), grant reference number: EP/m508196/1.

6 References

[1] L. Bárdoš. Radio frequency hollow cathodes for the plasma processing technology. *Surface and Coatings Technology*, 86-87(PART 2):648–656, 1996. ISSN 02578972. doi:10.1016/S0257-8972(96)03056-3.

[2] K. H. Schoenbach, R. Verhappen, T. Tessnow, F. E. Peterkin, and W. W. Byszewski. Microhollow cathode discharges. *Applied Physics Letters*, 13(1996):13, 1995. ISSN 00036951. doi:10.1063/1.116739.

[3] M. J. Kushner. Modeling of microdischarge devices: Pyramidal structures. *Journal of Applied Physics*, 95(3): 846–859, 2004. ISSN 00218979. doi:10.1063/1.1636251.

[4] R. Mavrodineanu. Hollow Cathode Discharges - Analytical Applications. *Journal of Research of the National Bureau of Standards*, 89(2):143, 1984. ISSN 0160-1741. doi:10.6028/jres.089.009.

[5] K. H. Schoenbach, A. El-habachi, W. Shi, and M. Ciocca. High-pressure hollow cathode discharges. *Plasma Sources Science and Technology*, 6:468–477, 1997. doi:10.1088/0963-0252/6/4/003.

[6] C. Lazzaroni, P. Chabert, A. Rousseau, and N. Sadeghi. Sheath and electron density dynamics in the normal and

self-pulsing regime of a micro hollow cathode discharge in argon gas. *European Physical Journal D*, 60(3):555–563, 2010. ISSN 14346060. doi:10.1140/epjd/e2010-00259-4.

[7] S. Dixon, C. Charles, R. W. Boswell, W. Cox, J. Holland, and R. Gottscho. Interactions between arrayed hollow cathodes. *Journal of Physics D: Applied Physics*, 46(14):145204, 2013. ISSN 0022-3727. doi:10.1088/0022-3727/46/14/145204.

[8] N. Schmidt, U. Czarnetzki, E. Schüngel, and J. Schulze. The effect of structured electrodes on heating and plasma uniformity in capacitive discharges. *Journal of Physics D: Applied Physics*, 46:505202, 2013. ISSN 0022-3727. doi:10.1088/0022-3727/46/50/505202.

[9] C. M. Horwitz. Hollow cathode etching and deposition. *Journal of Vacuum Science & Technology A: Vacuum, Surfaces, and Films*, 6(3):1837, 1988. doi:http://dx.doi.org/10.1116/1.575265.

[10] O. Taylan and H. Berberoglu. Dissociation of carbon dioxide using a microhollow cathode discharge plasma reactor: effects of applied voltage, flow rate and concentration. *Plasma Sources Science and Technology*, 24(1):015006, 2015. ISSN 0963-0252. doi:10.1088/0963-0252/24/1/015006.

[11] S. Takashima, M. Hori, T. Goto, A. Kono, M. Ito, and K. Yoneda. Vacuum ultraviolet absorption spectroscopy employing a microdiacharge hollow-cathode lamp for absolute density measurements of hydrogen atoms in reactive plasmas. *Applied Physics Letters*, 75(1999):3929, 1999. ISSN 00036951. doi:10.1063/1.125497.

[12] C. Charles, A. Bish, R. W. Boswell, J. Dedrick, A. Greig, R. Hawkins, and T. S. Ho. A Short Review of Experimental and Computational Diagnostics for Radiofrequency Plasma Micro-thrusters. *Plasma Chemistry and Plasma Processing*, 2015. ISSN 0272-4324. doi:10.1007/s11090-015-9654-5.

[13] R. A. Arakoni, J. J. Ewing, and M. J. Kushner. Microdischarges for use as microthrusters: modelling and scaling. *Journal of Physics D: Applied Physics*, 41(10):105208, 2008. ISSN 0022-3727. doi:10.1088/0022-3727/41/10/105208.

[14] L. Blackhall and J. Khachan. A simple electric thruster based on ion charge exchange. *Journal of Physics D: Applied Physics*, 40:2491–2494, 2007. ISSN 0022-3727. doi:10.1088/0022-3727/40/8/011.

[15] T. Lafleur and R. W. Boswell. Particle-in-cell simulations of hollow cathode enhanced capacitively coupled radio frequency discharges. *Physics of Plasmas*, 19(2), 2012. ISSN 1070664X. doi:10.1063/1.3685709.

[16] A. V. Phelps and Z. Lj. Petrovic. Cold-cathode discharges and breakdown in argon: surface and gas phase production of secondary electrons. *Plasma Sources Science and Technology*, 8(3):R21–R44, 1999. ISSN 0963-0252. doi:10.1088/0963-0252/8/3/201.

[17] B. G. Heil, U. Czarnetzki, R. P. Brinkmann, and T. Mussenbrock. On the possibility of making a geometrically symmetric RF-CCP discharge electrically asymmetric. *Journal of Physics D: Applied Physics*, 41(16):165202, 2008. ISSN 0022-3727. doi:10.1088/0022-3727/41/16/165202.

[18] H. Baránková and L. Bárdoš. Effect of gas and cathode material on the r.f. hollow cathode reactive PVD. *Surface and Coatings Technology*, 120-121:704–708, 1999. ISSN 02578972. doi:10.1016/S0257-8972(99)00362-X.

[19] Y. Ohtsu and Y. Kawasaki. Criteria of radio-frequency ring-shaped hollow cathode discharge using H2 and Ar gases for plasma processing. *Journal of Applied Physics*, 113(3), 2013. ISSN 00218979. doi:10.1063/1.4776220.

[20] Y. Ohtsu, N. Matsumoto, J. Schulze, and E. Schüngel. Capacitive radio frequency discharges with a single ring-shaped narrow trench of various depths to enhance the plasma density and lateral uniformity. *Physics of Plasmas*, 23(3), 2016. ISSN 10897674. doi:10.1063/1.4943964.

[21] K. J. Kanarik, T. Lill, E. A. Hudson, S. Sriraman, S. Tan, J. Marks, V. Vahedi, and R. A. Gottscho. Overview of atomic layer etching in the semiconductor industry. *Journal of Vacuum Science & Technology A: Vacuum, Surfaces, and Films*, 33(2):020802, 2015. ISSN 0734-2101. doi:10.1116/1.4913379.

[22] S. Samukawa, M. Hori, S. Rauf, K. Tachibana, P. Bruggeman, G. Kroesen, J. C. Whitehead, A. B. Murphy, A. F. Gutsol, S. Starikovskaia, U. Kortshagen, J.-P. Boeuf, T. J. Sommerer, M. J. Kushner, U. Czarnetzki, and N. Mason. The 2012 Plasma Roadmap. *Journal of Physics D: Applied Physics*, 45(25):253001, 2012. ISSN 0022-3727. doi:10.1088/0022-3727/45/25/253001.

[23] P. Chabert and N. Braithwaite. *Physics of Radio-Frequency Plasmas*. Cambridge University Press, Cambridge, 3rd edition, 2014.

[24] C. M. O. Mahony, R. Al Wazzan, and W. G. Graham. Sheath dynamics observed in a 13.56 MHz-driven plasma. *Applied Physics Letters*, 71(5):608, 1997. ISSN 00036951. doi:10.1063/1.119808.

[25] T Lafleur, P Chabert, and J P Booth. Secondary electron induced asymmetry in capacitively coupled plasmas. *Journal of Physics D: Applied Physics*, 46(13):135201, 2013. ISSN 0022-3727. doi:10.1088/0022-3727/46/13/135201.

[26] T Lafleur. Tailored-waveform excitation of capacitively coupled plasmas and the electrical asymmetry effect. *Plasma Sources Science and Technology*, 25(1):013001, 2016. ISSN 0963-0252. doi:10.1088/0963-0252/25/1/013001.

[27] E. Schüngel, D. Eremin, J. Schulze, T. Mussenbrock, and U. Czarnetzki. The electrical asymmetry effect in geometrically asymmetric capacitive radio frequency plasmas. *Journal of Applied Physics*, 112(5), 2012. ISSN 00218979. doi:10.1063/1.4747914.

[28] T Lafleur and J P Booth. Control of the ion flux and ion energy in CCP discharges using non-sinusoidal voltage waveforms. *Journal of Physics D: Applied Physics*, 45(39):395203, 2012. ISSN 0022-3727. doi:10.1088/0022-3727/45/39/395203.

[29] J. Schulze, E. Schüngel, U. Czarnetzki, and Z. Donko. Optimization of the electrical asymmetry effect in dual-frequency capacitively coupled radio frequency discharges: Experiment, simulation, and model. *Journal of Applied Physics*, 106(6), 2009. ISSN 00218979. doi:10.1063/1.3223310.

[30] J. K. Lee, O. V. Manuilenko, N. Yu. Babaeva, H. C. Kim, and J. W. Shon. Ion energy distribution control in single and dual frequency capacitive plasma sources. *Plasma Sources Science and Technology*, 14(1):89–97, 2005. ISSN 0963-0252. doi:10.1088/0963-0252/14/1/012.

[31] Z. Donkó, J. Schulze, B. G. Heil, and U. Czarnetzki. PIC simulations of the separate control of ion flux and energy in CCRF discharges via the electrical asymmetry effect. *Journal of Physics D: Applied Physics*, 42(2):025205, 2009. ISSN 0022-3727. doi:10.1088/0022-3727/42/2/025205.

[32] B. Bruneau, T. Novikova, T. Lafleur, J.-P. Booth, and E. V. Johnson. Control and optimization of the slope asymmetry effect in tailored voltage waveforms for capacitively coupled plasmas. *Plasma Sources Science and Technology*, 24:015021, 2015. ISSN 0963-0252. doi:10.1088/0963-0252/24/1/015021.

[33] B. Bruneau, T. Lafleur, T. Gans, D. O'Connell, A. Greb, I. Korolov, A. Derzsi, Z. Donkó, S. Brandt, E. Schüngel, J. Schulze, P. Diomede, D. J. Economou, S. Longo, E. Johnson, and J.-P. Booth. Effect of gas properties on the dynamics of the electrical slope asymmetry effect in capacitive plasmas: comparison of Ar, H_2 and CF_4. *Plasma Sources Science and Technology*, 25(1):01LT02, 2016. ISSN 0963-0252. doi:10.1088/0963-0252/25/1/01LT02.

[34] M. J. Kushner. Hybrid modelling of low temperature plasmas for fundamental investigations and equipment design. *Journal of Physics D: Applied Physics*, 42(19):194013, 2009. ISSN 0022-3727. doi:10.1088/0022-3727/42/19/194013.

[35] P. Tian and M. J. Kushner. Controlling VUV photon fluxes in low-pressure inductively coupled plasmas. *Plasma Sources Science and Technology*, 24:34017, 2015. ISSN 0963-0252. doi:10.1088/0963-0252/24/3/034017.

[36] M. A. Furman and M. T. F. Pivi. Probabilistic model for the simulation of secondary electron emission. *Physical Review Special Topics - Accelerators and Beams*, 5(12):82–99, 2002. ISSN 10984402. doi:10.1103/PhysRevSTAB.5.124404.

[37] S.-H. Song and M. J. Kushner. Control of electron energy distributions and plasma characteristics of dual frequency, pulsed capacitively coupled plasmas sustained in Ar and Ar/CF4/O2. *Plasma Sources Science and Technology*, 21 (5):55028, 2012. ISSN 0734-2101. doi:10.1088/0963-0252/21/5/055028.

[38] M. Hayashi. Report No. IPPJ-AM-19. Technical report, Nagoya Institute of Technology, 1991.

[39] K. Tachibana. Excitation of the $1s_5$, $1s_4$, $1s_3$ and $1s_2$ levels of argon by low-energy electrons. *Physical Review A*, 34(2), 1986. doi:10.1103/PhysRevA.34.1007.

[40] D. Rapp and P. EnglanderGolden. Total Cross Sections for Ionization and Attachment in Gases by Electron Impact. I. Positive Ionization. *The Journal of Chemical Physics*, 43(5):1464–1479, 1965. ISSN 0021-9606. doi:10.1063/1.1696957.

[41] N. A. Dyatko, Y. Z. Ionikh, I. V. Kochetov, D. L. Marinov, A. V. Meshchanov, A. P. Napartovich, F. B. Petrov, and S. A. Starostin. Experimental and theoretical study of the transition between diffuse and contracted. *J. Phys. D: Appl. Phys*, 41:055204, 2008. doi:10.1088/0022-3727/41/5/055204.

[42] A. Bogaerts, R. G. V. Serikov, and V. V. Serikov. Calculation of gas heating in direct current argon glow discharges. *Journal of Applied Physics*, 87, 1999. doi:10.1063/1.373545.

[43] H. W. Ellis, R Y Pai, E. W. Mcdaniel, E. A. Mason, and L. A. Viehland. Transport Properties of Gaseous Ions Over a Wide Energy Range. *Atomic Data and Nuclear Data Tables*, 17(3):177–210, 1976. doi:10.1016/0092-640X(76)90001-2.

[44] J. Schulze, E. Schüngel, U. Czarnetzki, M. Gebhardt, R. P. Brinkmann, and T. Mussenbrock. Making a geometrically asymmetric capacitive rf discharge electrically symmetric. *Applied Physics Letters*, 98(3):7–10, 2011. ISSN 00036951. doi:10.1063/1.3544541.